

The Abl/Enabled signaling pathway regulates Golgi architecture in *Drosophila* photoreceptor neurons

Ramakrishnan Kannan^a, Irina Kuzina^a, Stephen Wincovitch^b, Stephanie H. Nowotarski^c, and Edward Giniger^a

^aAxon Guidance and Neural Connectivity Unit, Basic Neuroscience Program, National Institute of Neurological Disorders and Stroke, and ^bCytogenetics and Microscopy Core, National Human Genome Research Institute, National Institutes of Health, Bethesda, MD 20892; ^cDepartment of Biology, University of North Carolina at Chapel Hill, Chapel Hill, NC 27599

ABSTRACT The Golgi apparatus is optimized separately in different tissues for efficient protein trafficking, but we know little of how cell signaling shapes this organelle. We now find that the Abl tyrosine kinase signaling pathway controls the architecture of the Golgi complex in *Drosophila* photoreceptor (PR) neurons. The Abl effector, Enabled (Ena), selectively labels the *cis*-Golgi in developing PRs. Overexpression or loss of function of Ena increases the number of *cis*- and *trans*-Golgi cisternae per cell, and Ena overexpression also redistributes Golgi to the most basal portion of the cell soma. Loss of Abl or its upstream regulator, the adaptor protein Disabled, lead to the same alterations of Golgi as does overexpression of Ena. The increase in Golgi number in *Abl* mutants arises in part from increased frequency of Golgi fission events and a decrease in fusions, as revealed by live imaging. Finally, we demonstrate that the effects of Abl signaling on Golgi are mediated via regulation of the actin cytoskeleton. Together, these data reveal a direct link between cell signaling and Golgi architecture. Moreover, they raise the possibility that some of the effects of Abl signaling may arise, in part, from alterations of protein trafficking and secretion.

Monitoring Editor

Richard Fehon
University of Chicago

Received: Feb 10, 2014

Revised: Jun 4, 2014

Accepted: Jul 29, 2014

INTRODUCTION

The Golgi apparatus, a central hub of the secretory pathway, is a highly dynamic, perinuclear organelle with distinct cellular architecture essential for coordinating plasma membrane trafficking events (Farhan and Rabouille, 2011; Cancino and Luini, 2013; Mayinger, 2013). Golgi morphology and localization are highly specialized and tailored to the needs of different cell types. In *Drosophila*, Golgi stacks are dispersed throughout the cytoplasm and reside in close

proximity to endoplasmic reticulum (ER) exit sites (Kondylis and Rabouille, 2003; Frescas *et al.*, 2006). Several Golgi-localized integral matrix proteins, including GRASPs (dGRASP65) and golgins (GM130, p115, Lava lamp, dGMAP, golgin-97, golgin-245, GCC-88 and GCC-185), aid to tether Golgi cisternae in both vertebrates and invertebrates (Kondylis and Rabouille, 2009). It remains obscure, however, how the unique biogenesis, morphology, and subcellular positioning of Golgi are established in neuronal cells and coordinated with the needs of development and physiology and what are the cellular signaling mechanisms engaged in this process.

A striking intimacy exists between cytoskeletal remodeling and the structural and functional organization of Golgi complex in different organisms (Kondylis and Rabouille, 2003; Egea *et al.*, 2006). Cytoskeletal filaments play a major role in regulating the dynamics and architecture of Golgi complex. The microtubule network is crucial to sustaining intracellular trafficking of the Golgi ribbon in mammals but does not control pairing of Golgi cisternae in *Drosophila* (Kondylis *et al.*, 2007). The golgin Lava lamp mediates dynein-dynactin based Golgi complex trajectories along microtubule tracks during *Drosophila* cellularization (Papoulas *et al.*, 2005), and,

This article was published online ahead of print in MBoC in Press (<http://www.molbiolcell.org/cgi/doi/10.1091/mbc.E14-02-0729>) on August 7, 2014.

Address correspondence to: Edward Giniger (ginigere@ninds.nih.gov).

Abbreviations used: CytoB, cytochalasin B; *dab^{mz}*, mutant of the gene *disabled* that is null both maternally and zygotically; ER, endoplasmic reticulum; EVH1, Ena/VASP homology domain 1; GFP, green fluorescent protein; LatD, latrunculin D; PBS, phosphate-buffered saline; PR, photoreceptor; RNAi, RNA interference; STED, stimulated emission depletion microscopy; WT, wild type.

© 2014 Kannan *et al.* This article is distributed by The American Society for Cell Biology under license from the author(s). Two months after publication it is available to the public under an Attribution–Noncommercial–Share Alike 3.0 Unported Creative Commons License (<http://creativecommons.org/licenses/by-nc-sa/3.0>).

“ASCB®,” “The American Society for Cell Biology®,” and “Molecular Biology of the Cell®” are registered trademarks of The American Society of Cell Biology.

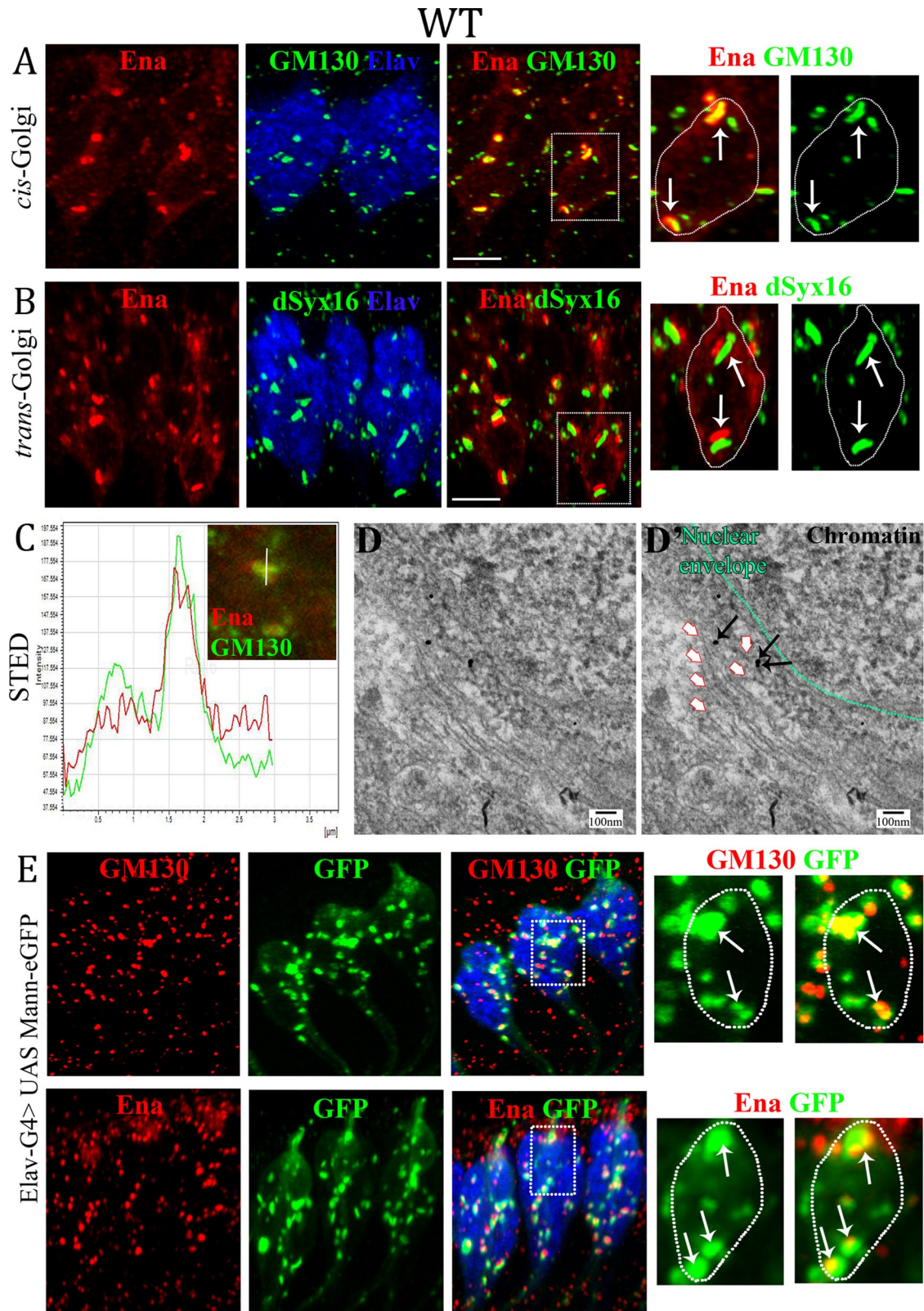


FIGURE 1: Enabled is a marker of the *cis*-Golgi compartment in wild-type larval photoreceptor (PR) neurons. (A, B) Eye disks of third-instar larvae were analyzed by immunofluorescence with the indicated markers. White boxed region is shown enlarged to the right of the respective panels. Irregular outlines in white highlight a single PR cell body. (A) Projected confocal micrograph of PR clusters stained for Ena (red), *cis*-Golgi marker GM130 (green), and Elav (to label PR nuclei; blue). Note that Ena-enriched structures in the PR cell body often colabel with the *cis*-Golgi marker GM130. Scale bar, 5 μ m. (B) Projected Z-stacks of PR cluster showing the relative distribution of Ena (red) with *trans*-Golgi marker dSyx16 (green). Ena structures were juxtaposed with *trans*-Golgi cisternae. Scale bar, 5 μ m. (C) Fluorescence intensity plot of a 3- μ m slice (white line in inset) across the *cis*-Golgi (green) in a single focal plane of a

conversely, stable Golgi complexes are potential sites for acen-trosomal microtubule nucleation (Ori-McKenney *et al.*, 2012). Recent evidence also strongly testifies to the role of an intact actin cytoskeleton in maintenance of Golgi architecture. Several key actin regulators localize to this organelle (Kondylis *et al.*, 2007; Salvarezza *et al.*, 2009; von Blume *et al.*, 2009, 2011; Colon-Franco *et al.*, 2011; Ori-McKenney *et al.*, 2012). Disruption of the Golgi-associated actin cytoskeleton leads to compact appearance of Golgi (Egea *et al.*, 2006) and alters selective protein trafficking and membrane remodeling (von Blume *et al.*, 2009, 2011; Almeida *et al.*, 2011). Disruption of Golgi structure, function, and localization, in turn, disturbs morphogenesis of neuronal projections in vivo (Ye *et al.*, 2007; Tong *et al.*, 2011) and in cell culture (Aridor *et al.*, 2009).

A central regulator of cellular actin dynamics is the nonreceptor cytoplasmic Abelson tyrosine kinase (Abl). Abl interacts with a spectrum of receptors at the plasma membrane to regulate remodeling of the neuronal cytoskeleton (Bashaw *et al.*, 2000; Colicelli *et al.*, 2010; Kuzina *et al.*, 2011; Gu *et al.*, 2012). Abl also controls cell shape, migration, epithelial integrity, polarity, hematopoiesis, and a variety of other developmental and physiological processes (Bradley and Koleske, 2009; Colicelli *et al.*, 2010). Abl executes many of its functions by suppressing the activity of the Ena/vasodilator-stimulated phosphoprotein (VASP) family of actin modulators: *Drosophila* Enabled (Ena), mammalian Mena, Evi, and VASP (Gertler *et al.*, 1990; Gates *et al.*, 2007). Ena/VASP proteins are direct targets of Abl kinase, and Abl also controls their distribution (Comer *et al.*, 1998; Krause *et al.*, 2002). Thus, in *Drosophila* epithelial morphogenesis, for example, a key function of Abl is to limit the scope of Ena action by controlling its subcellular localization (Gertler *et al.*, 1990; Grecengoed *et al.*, 2001, Grecengoed 2003). Ena proteins, in turn, regulate actin structure in at least three ways. They bundle actin filaments, promote actin polymerization directly, and inhibit capping of the fast-growing barbed ends of actin filaments (Hansen *et al.*, 2010). Several other cytoskeletal regulatory proteins and small GTPases have also been implicated in Abl-dependent developmental events, particularly Rac GTPase and its effectors (Liebl *et al.*, 2000; Grecengoed *et al.*, 2003; Gates *et al.*, 2007; Homem *et al.*, 2009; Hansen *et al.*, 2010; Lowery *et al.*, 2010; Song *et al.*, 2010). Thus Abl executes stringent control of downstream signaling events in a variety of developmental and physiological processes.

We now show that Abl/Ena signaling controls the subcellular architecture of the Golgi complex in *Drosophila* photoreceptor neurons through its regulation of the Golgi-associated actin cytoskeleton. We find that Ena selectively labels the *cis*-Golgi compartment in developing photoreceptors. Either overexpression or loss of Ena increases the number of *cis*- and *trans*-Golgi cisternae per cell, and Ena overexpression also causes a dramatic redistribution of Golgi to the most basal portion of the cell soma. Consistent with the known organization of the Abl/Ena signaling pathway, loss of function of either Abl or its upstream regulator, the adaptor protein Disabled (Song *et al.*, 2011), causes the same alterations of Golgi organization

as does overexpression of Ena. Live imaging reveals a constant flux of fissions and fusions of *cis*-Golgi cisternae in wild-type photoreceptors in vivo, and loss of Abl causes both an increase in the frequency of fission events and a decrease in fusions. Finally, using both genetic and pharmacological approaches, we show that the effects of Abl/Ena signaling on Golgi number and localization are mediated via their regulation of the actin cytoskeleton.

RESULTS

Enabled regulates Golgi complex in the photoreceptor cell body

We found that the Abl antagonist Ena is associated with the *cis*-Golgi compartment in wild-type *Drosophila* photoreceptor (PR) neurons (Figure 1, A and C–E). In late third-instar eye imaginal disks, Ena is localized in three subcellular compartments in PR neuronal cell bodies. These are 1) actin-rich apical microvilli-like structures that at later stages develop into mature rhabdomeres; 2) the cortical actin cytoskeleton, which shows diffuse and uniform accumulation of Ena; and 3) distinct perinuclear flattened structures in the cytoplasm. We found strong colabeling of these Ena-enriched flattened structures with GM130, a bona fide marker for the *cis*-Golgi compartment of the Golgi complex (Figure 1A). Approximately 72.2% ± 1.0 (percent ± SEM) of Ena puncta were associated with GM130 *cis*-Golgi structures ($n = 769$ puncta from 11 wild-type disks). Ena structures do not show obvious overlap with other endomembrane compartments, such as early endosomes (Rab5-GFP), late endosomes and lysosomes (Rab11), or centrosomes (CNN–green fluorescent protein [GFP]; unpublished data).

We confirmed the association of Ena with the *cis*-Golgi by two independent approaches. First, in agreement with the foregoing observations, we found that Ena structures colocalized with GFP fusions to a *cis*-Golgi resident protein, α -mannosidase II (Figure 1E). Second, we used an antibody that labels the *trans*-Golgi compartment of the Golgi complex, anti-dSyntaxin-16 (dSyx-16), to examine the relationship between Enabled distribution and the *trans*-Golgi (Xu *et al.*, 2002). In contrast to the *cis*-Golgi marker, we found that the *trans*-Golgi marker dSyx-16 labeled puncta that were adjacent to Ena structures but showed no significant overlap (Figure 1B). To further improve our resolution of Golgi structures, we used superresolution stimulated emission depletion (STED) microscopy, which offers lateral resolution of 80–100 nm, as compared with 240–450 nm for standard confocal approaches. By STED, as by traditional confocal microscopy, we observed strong colabeling of Ena with *cis*-Golgi structures in wild-type larval PR (Figure 1C; also see later discussion of Figure 4D). Finally, transmission immuno–electron microscopy with anti-Ena antibodies reproducibly revealed anti-Ena-gold signal associated with the *cis* portion of morphologically recognizable Golgi structures (Figure 1, D and D'), as well as in other regions of the cell where Ena protein is expected to be found (e.g., along the plasma membrane at the cell cortex).

two-color STED micrograph. Note the close agreement between Ena (red) and *cis*-Golgi (green) at a lateral resolution of ~100 nm. (D) Immuno–electron micrograph of wild-type eye disk. (D') Same image with key features marked. Black arrows indicate anti-Ena antibody labeling detected with Nanogold secondary (dense black dots). Open white arrowheads highlight Golgi cisternae. Nuclear envelope (dotted cyan line) and chromatin are indicated for reference. Note that the classic appearance of Golgi as thin, stacked leaflets applies primarily to the medial and *trans* compartments, whereas the *cis*-Golgi tends to be thicker and more irregular. Scale bar, 100 nm. Image was collected at 30,000× magnification. (E) Elav-G4>UAS- α -mannosidase II-eGFP. Top row: Tissue stained for GM130 (red), GFP (green), and Elav for PR nuclei (blue). As expected, α -mannosidase II-eGFP colocalized extensively but not perfectly with anti-GM130 (Zuber *et al.*, 2000). Bottom row: Ena in red, GFP in green, and Elav for PR nuclei in blue. Scale bar, 5 μ m.

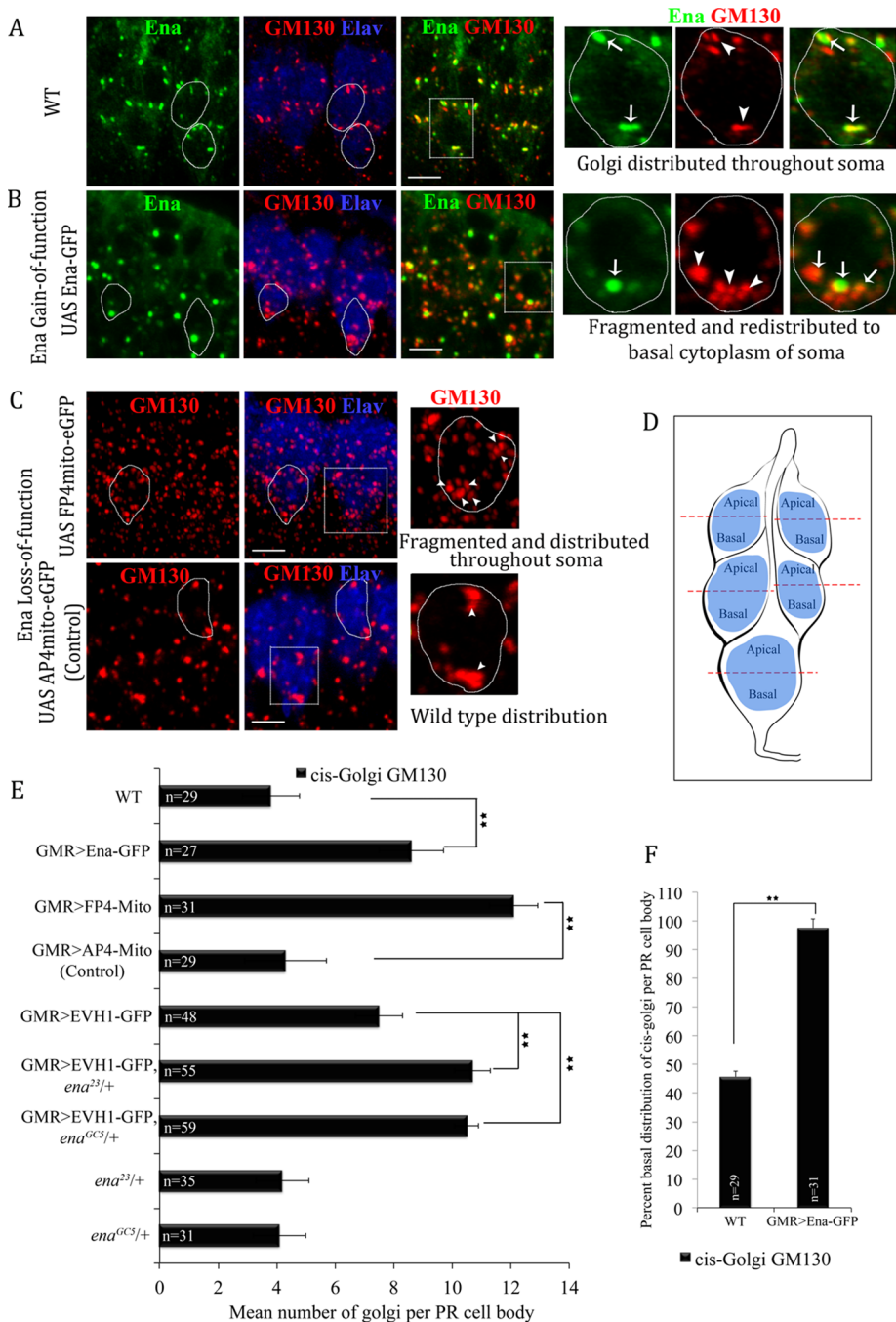


FIGURE 2: *cis*-Golgi complex is sensitive to the levels of Enabled protein. (A–C) Z-projections of confocal stacks of mature PR clusters labeled for Ena (green), *cis*-Golgi (GM130, red) and PR nuclei (Elav, blue). Individual PR cell bodies are traced (irregular white outlines). White boxes indicate regions shown enlarged to the right. Arrows point to Ena puncta; arrowheads point to GM130 puncta. Scale bar, 5 μ m. (A) In wild type, Ena and *cis*-Golgi puncta are scattered throughout the cytoplasm of each PR cell body. (B) Ena overexpression relocates endogenous and expressed Ena to the basal end of PR cell body. Also note an increase in the number and accumulation of *cis*-Golgi cisternae in the vicinity of the accumulated Ena. Typically Ena accumulates to very high levels in one large basal punctum, whereas lower levels of Ena are detected in association with the other basal cisternae. (C) Ena loss of function (FP4-mito) increases the number of *cis*-Golgi cisternae throughout the PR cell body, whereas GM130 in control (AP4-mito) resembles WT (A). (D) Scheme used to quantify apicobasal distribution. Puncta were counted separately in the apical and basal halves of each photoreceptor. Data are expressed as puncta located in the basal halves of the cells as a percentage of the total. (E) Quantification of *cis*-Golgi fragmentation phenotypes. *n* is indicated on the bars; error bars represent SEM. Statistical significance by ANOVA (***p* < 0.001). (F) *cis*-Golgi distribution in basal region of PR cell was quantified. *n* is indicated on the bars; error bars represent SEM. *p* values were calculated by ANOVA (***p* < 0.001).

The number and subcellular distribution of Golgi cisternae were profoundly sensitive to the level of Ena protein (Figures 2, A–F, and 3, D and E). In WT we found 3.8 ± 1.0 *cis*-Golgi cisternae (GM130 positive; mean \pm SEM) and 5.5 ± 1.2 *trans*-Golgi (dSyx-16 positive) per PR cell body scattered more or less evenly across the soma (Figures 2, A and E, and 3, A and F), with $45.6\% \pm 2.1$ of *cis*-Golgi and $50.3\% \pm 1.9$ of *trans*-Golgi in the basal half of the cell and the rest apical (Figures 2F and 3G). In contrast, when we overexpressed an Ena-GFP fusion, the number of distinguishable cisternae increased dramatically (to 8.6 ± 1.1 *cis*-Golgi, *p* = 2.1×10^{-5} ; and 15.7 ± 0.9 *trans*-Golgi; *p* = 2.7×10^{-4} ; Figures 2E and 3F), and the cisternae overwhelmingly relocated to the most basal part of the cell soma, near the axon exit point (*cis*-Golgi, $97.5\% \pm 3.3$ basal, *p* = 2.3×10^{-4} ; and *trans*-Golgi, $79\% \pm 4.6$ basal; *p* = 2.6×10^{-5} ; Figures 2F and 3G). Both the expressed and the endogenous Ena relocated in concert with the Golgi, coalescing at the most basal point of the cell soma (Figures 2B and 3D). We verified that the phenotype from *ena* overexpression was formally a genetic gain of function by showing that the severity of the phenotype was quantitatively reduced by heterozygosity for the endogenous *ena* locus (Figure S2, D and E).

Reduction of functional Ena also caused an increase in Golgi number (Figures 2C and 3E). Because zygotic *ena* mutants die before reaching larval stage and we were unable to recover PR cell clones homozygous for the strong *ena* mutant alleles *ena²³* and *ena²¹⁰* (R.K. and E.G., unpublished data), we reduced *ena* function by expressing UAS-FP4-eGFP-mito to sequester Ena at mitochondria (Bear *et al.*, 2002; Gates *et al.*, 2007, 2009; Grevengoed *et al.*, 2003). UAS-AP4-eGFP-mito, which does not bind Ena, was a specificity control. We detected 12.1 ± 0.8 *cis*-Golgi and 14.2 ± 0.7 *trans*-Golgi structures in Ena loss of function (FP4-mito) compared with 4.3 ± 1.4 *cis*-Golgi and 6.3 ± 0.7 *trans*-Golgi structures in control (AP4-mito) (Figure 2, C and E). We verified that expression of FP4-mito produces a genetic loss of function for *ena* by showing that its phenotype is enhanced by heterozygosity for the endogenous *ena* locus (Supplemental Figure S2F). Moreover, we showed by immunofluorescence that the endogenous Ena protein is recruited to the expressed FP4-mito (Supplemental Figure S2, A–C).

We next sought an independent manipulation to verify the effect of *ena* loss of function on Golgi organization. Unfortunately, the available *ena* RNA interference (RNAi) reagents failed to reduce the level of Ena protein significantly in eye disk. It is

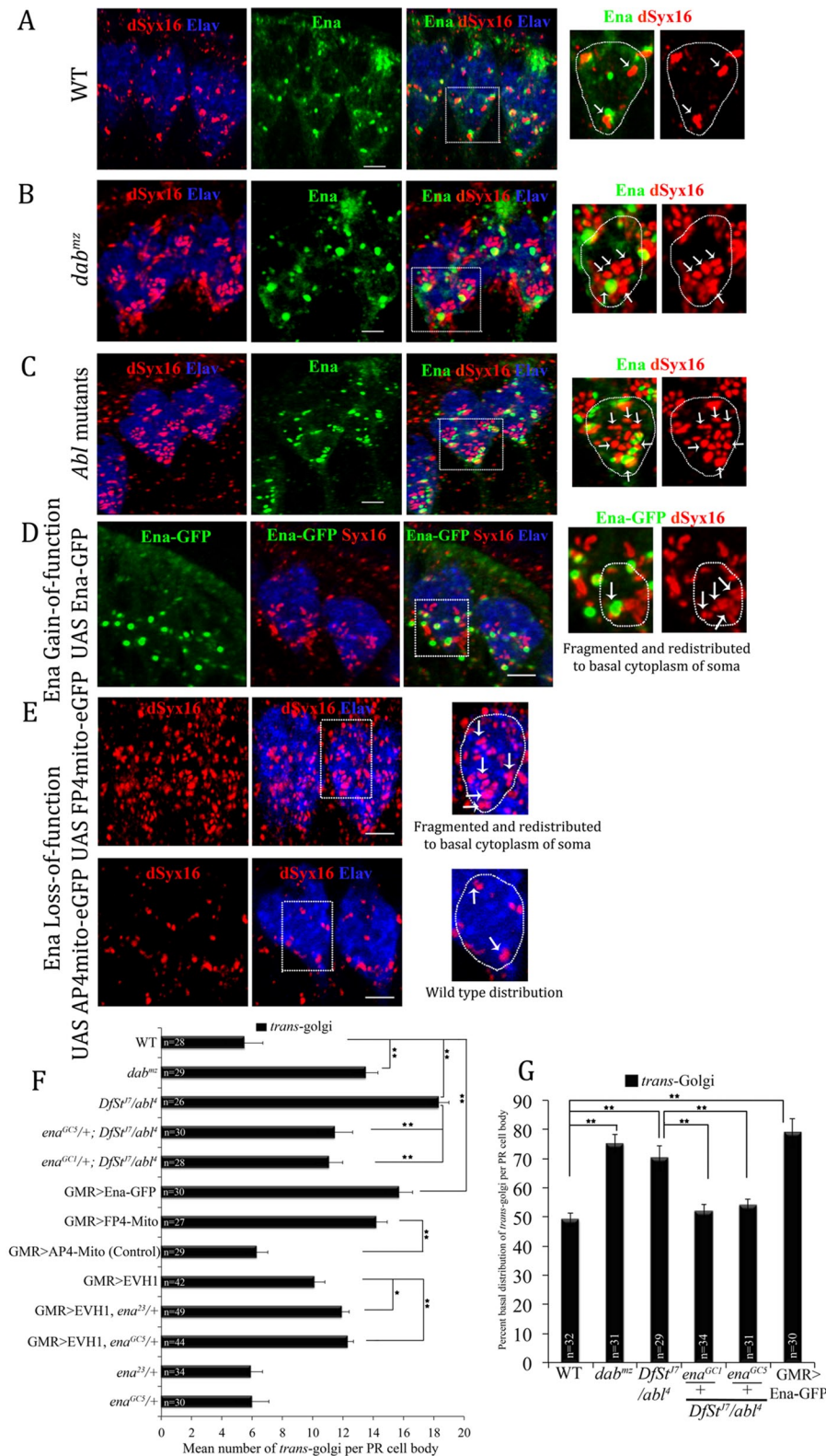


FIGURE 3: Control of *trans*-Golgi organization and distribution by Abl/Ena signaling pathway. (A–E) Projected Z-stacks of confocal micrographs of third-instar larval eye disks stained for Ena or Ena-GFP (green), *trans*-Golgi (dSyx16, red), and PR nuclei (Elav, blue). White boxes indicate regions shown enlarged to the right. Single PR cell body is traced (irregular white outlines) in enlarged panels. Arrows point to localization of Ena and dSyx16 puncta. Scale bar, 5 μ m. (A) Wild type. (B) *dab^{mz}*. (C) *Df st¹⁷/abl¹*. (D) GMR>UAS Ena-GFP. (E) Ena loss-of-function GMR>UAS FP4-mito-eGFP and GMR> UAS AP4-mito-eGFP (control). (F) Quantification of *trans*-Golgi structures in a single PR cell body. (G) Quantification of percentage basal distribution of

often the case that expression of one domain of a multifunctional protein acts as a dominant negative (Herskowitz, 1987). We reasoned that overexpression of just the localization domain of Ena (EVH1), in the absence of the actin-regulatory portions of the protein, would interfere with the function of the endogenous protein. Indeed, we found that expressed EVH1-GFP localized in a pattern indistinguishable from that of endogenous Ena but induced an increase in the number of Ena puncta and of Golgi puncta, just as did expression of FP4-mito (7.5 ± 0.8 *cis*- and 10.1 ± 0.7 *trans*-Golgi structures per cell, respectively). We further verified that this represented a loss-of-function condition for *ena* by reducing the endogenous *ena* by 50% with a heterozygous mutation and demonstrating that this enhanced the EVH1-overexpression phenotype. Thus EVH1 overexpression together with heterozygous *ena* loss of function yielded 10.7 ± 0.6 *cis*- ($p = 1.5E-07$) and 11.9 ± 0.5 *trans*-Golgi ($p = 0.015$) per cell body in EVH1,*ena²³/+* and 10.5 ± 0.4 *cis* ($p = 1.1E-02$) and 12.3 ± 0.3 *trans*-Golgi ($p = 1.8E-04$) in EVH1,*ena^{GCS}/+* (Figures 2E and 3F). Heterozygosity for *ena* by itself did not alter Golgi number (Figures 2E and 3F).

Activity of the Abl tyrosine kinase pathway controls Golgi distribution

In light of the striking effects of Ena on Golgi morphology we investigated Golgi structure in embryos mutant for other components of the Abl signaling pathway. We found that both *dab^{mz}* and *Abl* mutations caused Golgi fragmentation and redistribution to basal cytoplasm, similar to that produced by overexpression of Ena, both by confocal (Figures 4, A–C, and 3, A–C) and STED microscopy (Figure 4, D–F). In *dab*-null mutants we detected 10.2 ± 1.5 *cis*-Golgi structures per cell, with 87.6 ± 2.5 in the basal portion of the cell, and 13.5 ± 1.9 *trans*-Golgi structures, with 75.2 ± 3.2 basal. Similarly, *Abl* zygotic mutants showed a significant increase in the fragmentation state of *cis*-Golgi (15.8 ± 1.9) and *trans*-Golgi (18.3 ± 1.0) and basal redistribution of Golgi stacks in the cell body (*cis*-Golgi, 75.5 ± 3.9 basal; and *trans*-Golgi, 70.3 ± 4.2 basal (Figures 4, G and H, and 3, F and G). In both mutants, the basal accumulation of Golgi was accompanied by basal accumulation of the endogenous Ena. The basal accumulations

trans-Golgi structures in a single PR cell body. *n* for each genotype is reported on the bars. Error bars represent SEM. ** $p < 0.001$ and * $p < 0.05$.

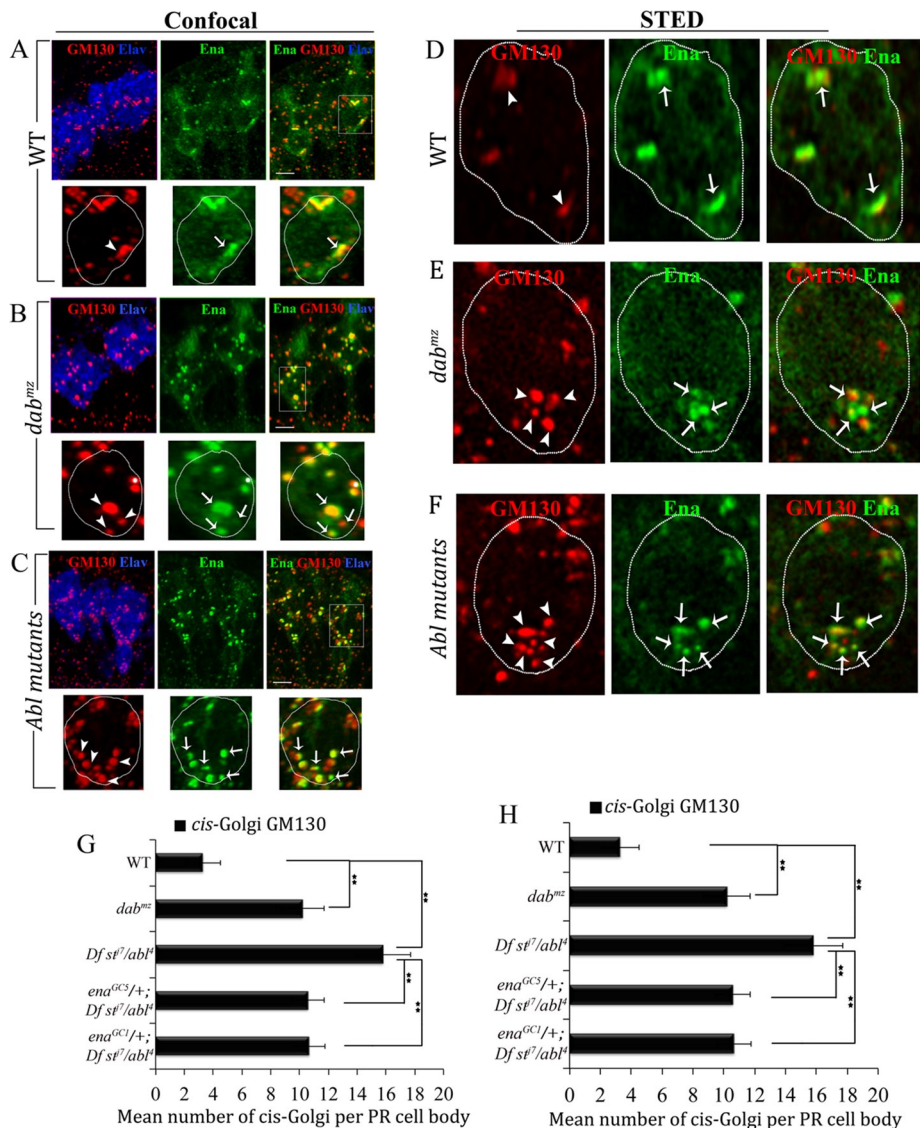


FIGURE 4: Abl signaling pathway controls *cis*-Golgi organization and distribution. (A–C) Projected confocal Z-stacks of larval eye disks stained with the indicated antibodies. (A) Wild type. (B) *dab^{mz}*. White asterisks in enlarged panels correspond to GM130 and Ena puncta from a neighboring cell body in the PR cluster. (C) *Abl* mutant (*Df st⁷/abl⁴*). Note that in the *dab* and *Abl* mutants the number of both Ena- and GM130-positive puncta in each cell is increased, and they are preferentially redistributed to the basal cytoplasm of each cell. (D–F) Single optical sections of WT (D), *dab^{mz}* (E), and *Df st⁷/abl⁴* (F) larval eye disks acquired through STED microscopy (GM130 in red and Ena in green). (G) Quantification of *cis*-Golgi fragmentation phenotypes in WT, *dab^{mz}*, and *Abl* mutants. *n* is reported on the bars. *p* values were calculated by ANOVA (***p* < 0.001). Error bars represent SEM. (H) Quantification of *cis*-Golgi distribution in WT and *Abl* pathway mutants. *n* for each genotype is reported on the bars. Error bars represent SEM. ***p* < 0.001.

of Ena and of Golgi were somewhat less complete and observed at lower expressivity in *Abl* mutants than in *dab^{mz}*. In part, this is likely because the *dab^{mz}* mutant lacks all Disabled protein both maternally and zygotically (Song *et al.*, 2010), whereas functionally significant amounts of maternal Abl product appear to persist in eye disks of this stage in *Abl* zygotic mutants (R.K. and E.G., unpublished data). We did not observe gross disruption of overall actin organization in either mutant, although we could not rule out more subtle effects on cytoskeletal dynamics. We observed similar effects on Golgi distribution by expressing UAS-Abl RNAi in all cells posterior to the morphogenetic furrow (GMR-G4) or only in mature PR neurons

(Elav-G4), suggesting that the effect of Abl on Ena and Golgi is cell autonomous (Figure S1, A–H). As expected, the *Abl* mutant phenotype was suppressed by heterozygosity for *ena*, as is true of all other characterized *Abl* phenotypes (Figure 4, G and H).

Abl tyrosine kinase controls Golgi fragmentation by regulating the dynamics of fission and fusion events

Live imaging of Golgi biogenesis using a Golgi marker, α -mannosidase II-eGFP, revealed that Abl controls the dynamics of Golgi fusion and fission events in vivo (Figure 5, A–C, and Supplemental Movies S1 and S2). In wild-type PR neurons, small clusters consisting of vesicular and tubular-shaped Golgi structures were present throughout the cell. They were highly dynamic and exhibited stochastic movement in both apical and basal directions. We also observed selective fusion of neighboring vesicular structures, eventually leading to the formation of tubular-shaped Golgi, as well as to fission of preexisting Golgi structures (Figure 5A and Supplemental Movie S1). Fusion and fission events were not synchronous for all Golgi structures in the same cell. In *Abl* mutants (Figure 5B and Supplemental Movie S2), Golgi exhibit restricted movement compared with the dynamics observed in wild type (Figure 5A), with Golgi puncta staying more aggregated in the vicinity of their neighbors. Moreover, counting fission and fusion events revealed a significant increase in fission and decrease in fusion of Golgi fragments per unit time in *Abl* mutants compared with wild type. In WT eye disks, we observed 3.6 ± 0.8 apparent fission events and 4.9 ± 0.3 fusion events per PR cluster per 15.6-s observation period (as assessed morphologically, at the resolution of spinning disk confocal imaging). In contrast, *Abl* mutants showed 6.8 ± 0.4 apparent fission events ($p = 1.8E-07$) and 2.4 ± 0.9 fusion events per cluster ($p = 2.1E-08$). Thus it appears that Abl activity promotes fusion and limits fission of Golgi fragments in PR neurons (Figure 5C).

Abl tyrosine kinase pathway controls Golgi distribution through regulation of actin structure

Genetic and pharmacological experiments suggest that Abl/Ena signaling controls Golgi distribution through its regulation of the actin cytoskeleton. Ena promotes actin filament assembly in part by blocking capping of the barbed ends of actin filaments (Bear *et al.*, 2002). Thus capping protein- β (*cpb*) and Ena act antagonistically during *Drosophila* oogenesis (Gates *et al.*, 2009) and axon patterning (Kuzina *et al.*, 2011), with *cpb* genetically downstream of *ena* (Gates *et al.*, 2009). We found that promoting actin capping by co-expressing *cpb* with *ena* significantly suppressed Ena-dependent

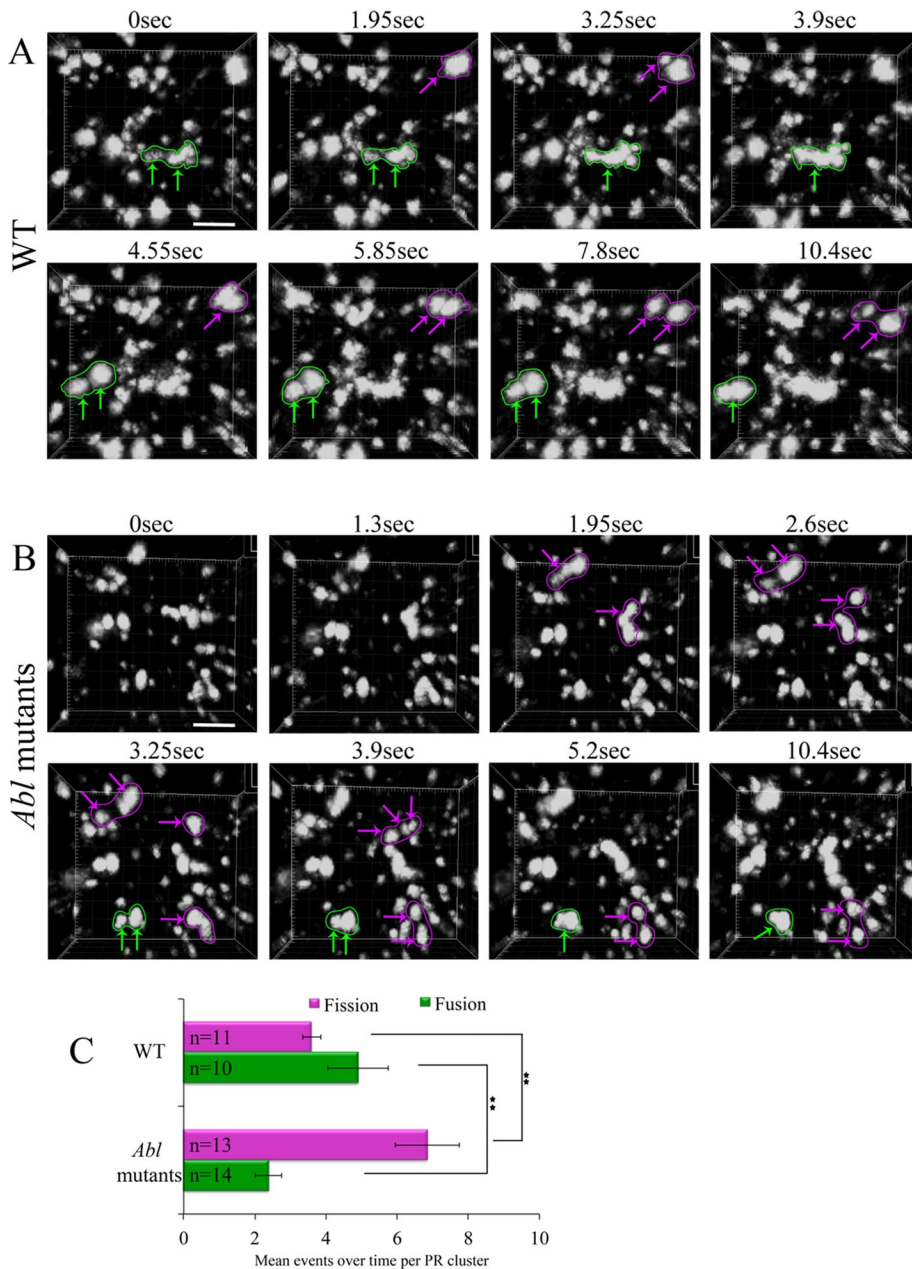


FIGURE 5: Abl regulates fusion and fission of Golgi fragments in larval photoreceptor neurons. (A, B) Representative single Z-slices acquired during live imaging of Golgi dynamics in third-instar larval PR neurons, using an α -mannosidase-eGFP reporter. Examples of fusion events are circled in green; examples of fission events are circled in purple. Images were obtained by spinning disk confocal microscopy, with images collected every 0.65 s over an imaging period. Scaling per pixel: $0.21 \times 0.21 \times 1 \mu\text{m}$. Note that individual cisternae move in or out of the plane of focus at some time points. (A) Wild type. (B) *Abl* mutant (*Df st^{J7}/abl⁴*). For additional data, see also Supplemental Movies S1 and S2. (C) Quantification of fission and fusion events over a 15.6-s time period in one PR cluster in WT and *Abl* mutants. Statistical significance evaluated by ANOVA. ** $p < 0.001$. Error bars represent SEM. Note that the histogram presents the number of Golgi cisternae per PR cluster, not per cell.

basal accumulation of *cis*-Golgi (UAS-Ena, $98.3\% \pm 1.8$ basal, vs. UAS-*cpb* + UAS-Ena, $43.8\% \pm 2.6$ basal; not significantly different from WT, $43.4\% \pm 4.2$ basal; Figure 6, A–C). Enhanced capping also suppressed Ena-dependent fragmentation of *cis*-Golgi cisternae in PR (UAS-Ena, 8.9 ± 1.3 fragments, vs. UAS-*cpb* + UAS-Ena, 3.9 ± 1.5 fragments; not significantly different from WT, 3.3 ± 1.0 fragments) (Figure 6F). Ena localization was also largely restored to the wild-

type pattern by coexpressing *cpb* with *ena* (Figure 6B) compared with *ena* gain-of-function alone (Figure 6A). Overexpression of capping protein alone did not show any significant effects on Golgi distribution or Ena localization (Figure 6C), and co-overexpression of *cpb* did not noticeably alter the level of UAS-driven *ena* (as assessed by fluorescence intensity).

Time-resolved pharmacological experiments further confirmed that Abl controls Golgi distribution through actin regulation (Figure 7, A–H). Third-instar larval eye disks were cultured for 1 h in media containing low concentrations of the actin depolymerizing agent cytochalasin B (CytoB; Figures 7, A–C) or latrunculin D (LatD; Figure 7, F–H) to select a concentration that reduced phalloidin staining but did not alter the overall morphology of PR. In WT, CytoB treatment fragments the *cis*-Golgi compartment without altering its apical-basal distribution (Figure 7A). These effects resemble Golgi phenotypes observed in Ena loss of function (Figure 2C). We then tested whether pharmacological disruption of actin structure modified the basal redistribution of *cis*-Golgi in *dab^{mz}* (Figure 7B) and *Abl* mutants (Figure 7C). In mock-treated control cultures, we observed a high percentage of basally distributed *cis*-Golgi structures in *dab^{mz}* ($90.4\% \pm 6.1$) and in *Abl* mutants ($77.3\% \pm 5.7$) compared with WT ($60\% \pm 4.8$; Figure 7D). Acute treatment with CytoB ($20 \mu\text{M}$) significantly restored the WT apical-basal distribution of *cis*-Golgi structures in *dab^{mz}* ($64\% \pm 6.4$) and in *Abl* mutant ($61.3\% \pm 4.9$), respectively (Figure 7D). These data imply, first, that formation and maintenance of the basal redistribution of Golgi in *Abl* pathway mutants is an active process unleashed by derepression of Ena, and, second, that actin structure is functionally downstream of Abl/Ena activity for Golgi distribution. We also observed a synergistic increase in the mean number of *cis*-Golgi fragments in drug-treated *dab^{mz}* (14.7 ± 1.8) and *Abl* mutant (18.9 ± 1.8) tissues compared with their respective mutant mock control alone (*dab^{mz}*, 9.9 ± 1.4 ; *Abl*, 13.1 ± 1.3 ; Figure 7E). Comparable results were obtained with LatD-treated (10 mM) eye disk cultures (Figure 7, F–J). Taken together, these results suggest that the effects of the Abl/Ena pathway on Golgi localization, and probably on Golgi fragmentation, are mediated through

regulation of actin dynamics. Consistent with this, in WT eye disks, we often detected enriched F-actin foci adjacent to *cis*-Golgi structures (Figure 6D).

DISCUSSION

We found that the Abl tyrosine kinase signaling pathway controls Golgi morphology and localization in *Drosophila* photoreceptors

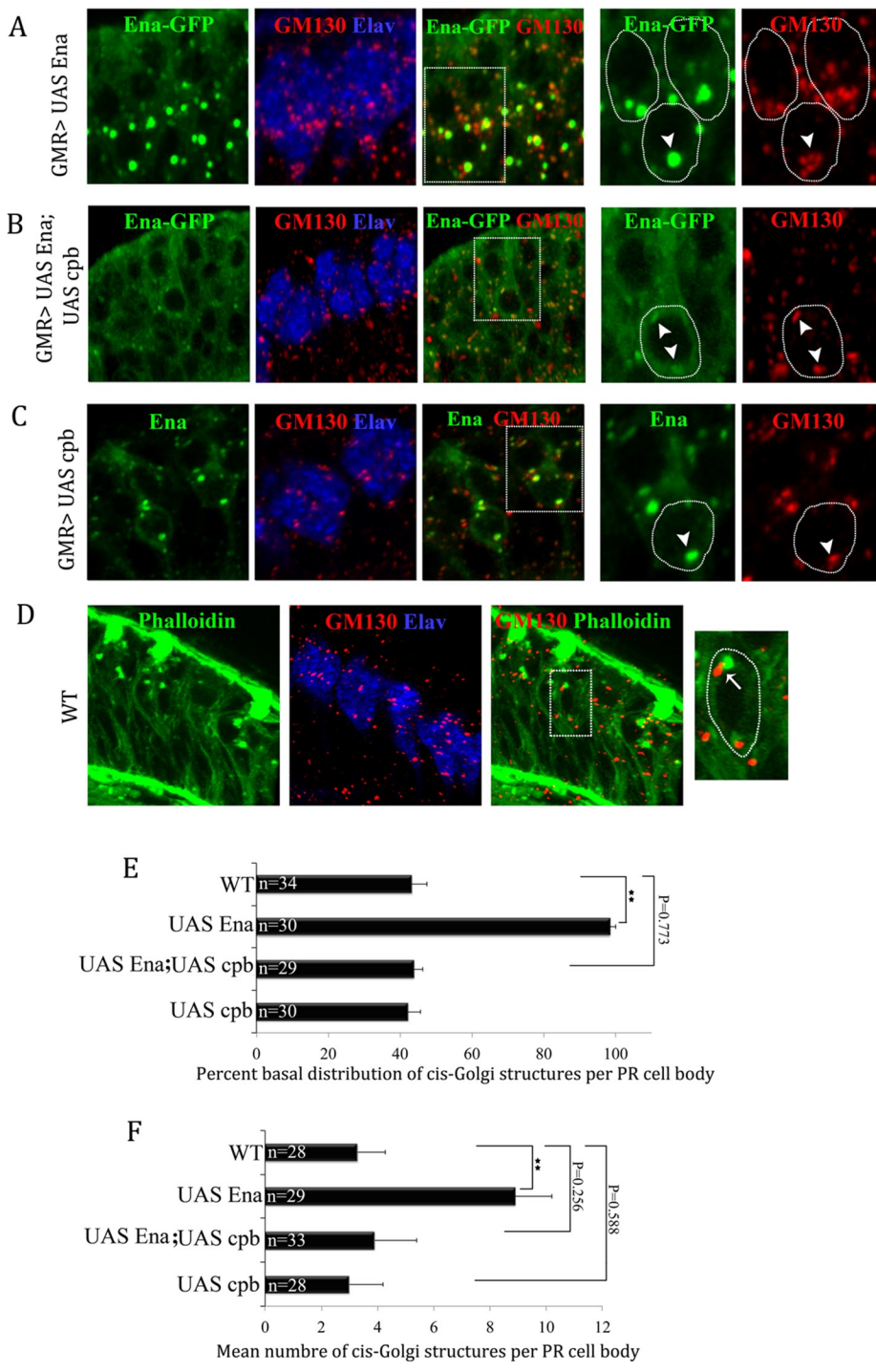


FIGURE 6: Coexpression of cpb and Ena rescues *cis*-Golgi phenotypes. (A) Overexpression of Ena alone. (B) Coexpression of Ena and cpb. (C) Overexpression of Cpb alone. Note that overexpression of cpb suppresses both fragmentation and basal localization of Golgi puncta and of Ena itself. (D) Single optical section of a wild-type eye disk stained for F-actin (phalloidin; green) and *cis*-Golgi (anti-GM130; red). Note accumulation of F-actin adjacent to many Golgi puncta. Some of the Golgi are adjacent to actin foci not visible in this focal plane. Elav (blue) marks PRs. (E) Quantification of Golgi apicobasal distribution for Ena and cpb coexpression experiment (A–C). (F) Quantification of Golgi fragmentation for Ena and Cpb coexpression experiments (A–C). *n* for each genotype is reported on the bars. Error bars represent SEM. ***p* < 0.001.

through its regulation of the actin cytoskeleton. Ena, the main effector of Abl in morphogenesis, is associated with the *cis*-Golgi compartment, and it regulates Golgi localization and dynamics under

fragmentation of preexisting Golgi cisternae and not to de novo synthesis of Golgi. First, our live imaging of Golgi dynamics in neurons of the *Drosophila* eye disk reveals that the steady-state number

the control of Abl and its interacting adaptor protein, Dab. Reducing the levels of Abl or Dab or overexpressing Ena led to similar defects in Golgi fragmentation state and subcellular distribution. During Golgi biogenesis, Abl increases the frequency of fusion of Golgi cisternae and decreases fission events. Abl evidently controls Golgi organization through its regulation of actin structure, as the effect of Abl signaling on Golgi could be blocked by modulating actin structure genetically or pharmacologically. Collectively these data reveal an unexpected link between a fundamental tyrosine kinase signaling pathway in neuronal cells and the structure of the Golgi compartment.

Abl signaling, actin structure, and Golgi organization

The data reported here suggest that the Abl signaling pathway controls Golgi morphology and localization through its control of actin structure. This is consistent with previous reports that altering the levels of actin modulators perturbs the structure and function of the Golgi apparatus (Camera *et al.*, 2003; Rosso *et al.*, 2004; Egea *et al.*, 2006). A variety of proteins that modulate actin dynamics have been localized to Golgi (Matas *et al.*, 2004; Gomez and Billadeau, 2009; Salvarezza *et al.*, 2009; von Blume *et al.*, 2009; Anitei *et al.*, 2010; Colon-Franco *et al.*, 2011). Ultrastructural studies established the association of actin filaments with Golgi membranes and the association of β and γ -actin with the Golgi (Valderrama *et al.*, 2000). In cultured cell models, including neurons, actin depolymerization leads to Golgi compactness, fragmentation, and altered subcellular distribution (Camera *et al.*, 2003; Rosso *et al.*, 2004). We note, moreover, that the reported Golgi-associated signaling proteins include several that have been linked to Abl signaling, including the Abl target Abi, the Abi binding partner WAVE, and various effectors of Rac GTPase, including ADF/cofilin, WASH, and Arp2/3. Thus, for example, Abi and WAVE have been implicated in actin-dependent Golgi stack reorganization and in scission of the Golgi at cell division to allow faithful inheritance of Golgi complex to daughter cells in *Drosophila* S2 cell cycles (Kondylis *et al.*, 2007). These data reinforce the importance of actin-regulating signaling pathways for controlling Golgi biogenesis.

Two lines of evidence suggest that the increase we observe in Golgi number in Abl pathway mutants is due primarily to net

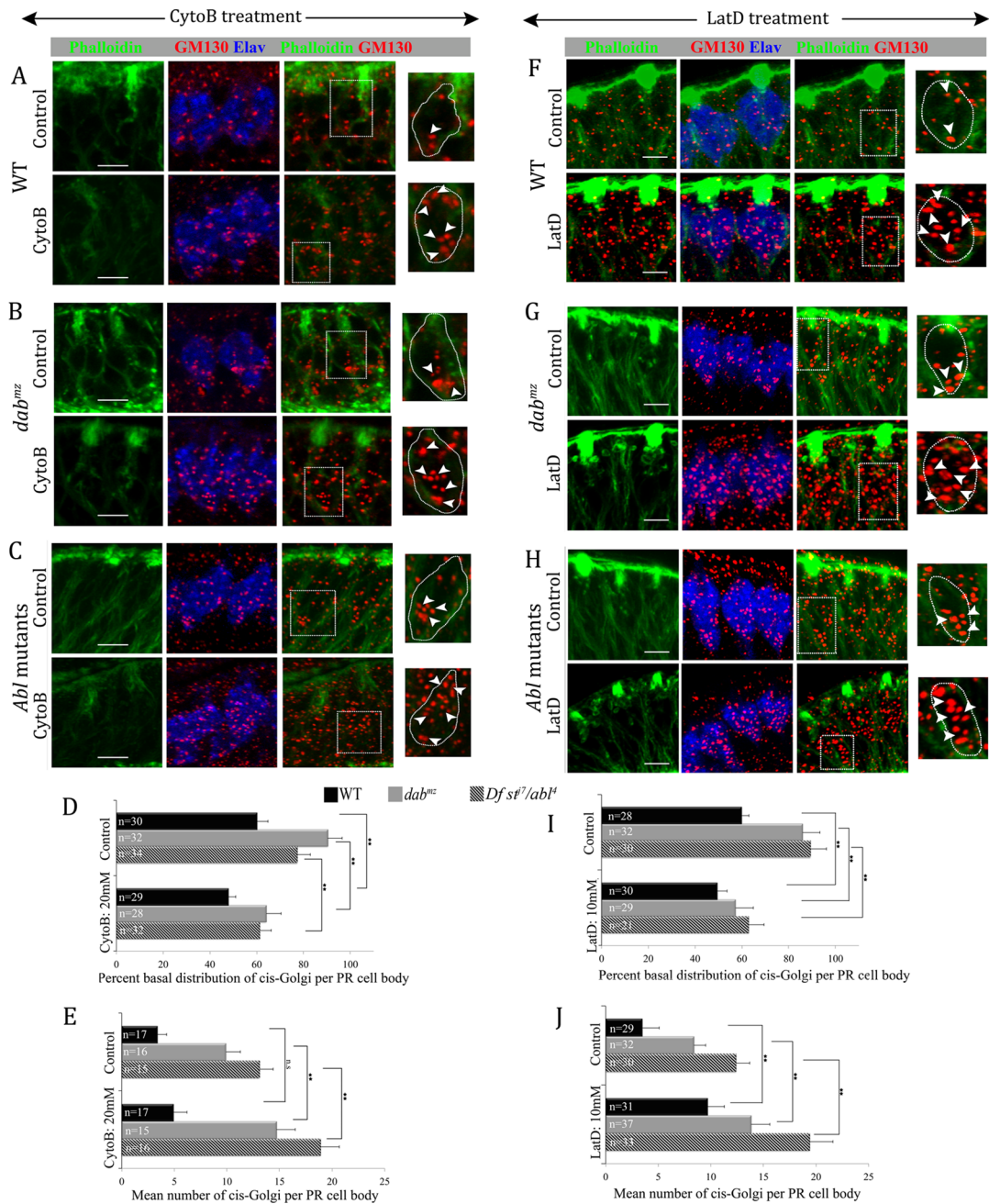


FIGURE 7: Pharmacological disruption of actin structure is downstream of Abl signaling for Golgi distribution. (A–C) Confocal imaging of third-instar eye imaginal disks cultured in 20 mM cytochalasin B and mock-treated controls, stained for phalloidin (green), *cis*-Golgi (anti-GM130; red), and anti-Elav (blue). All sections were acquired at similar settings. Note the decrease in phalloidin staining at the cortex in CytoB-treated cultures compared with mock controls. A single PR cell body is outlined in enlarged panels for the various conditions. Arrowheads highlight *cis*-Golgi cisternae. (A) WT. (B) *dab^{mz}*. (C) *Abl* mutant (*Df st^{J7}/abl^{l4}*). Note that Golgi cisternae are concentrated in the basal cytoplasm in the mock-treated mutants but become randomized throughout the cell upon treatment with CytoB. (D, E) Quantification of CytoB-epistasis data. *n* for each experiment is reported on the bars. Error bars correspond to SEM. *****p* < 0.001** (ANOVA). (D) Quantification of *cis*-Golgi distribution after CytoB-mediated disruption of actin polymerization in WT, *dab^{mz}*, and *Abl* mutant (*Df st^{J7}/abl^{l4}*) eye disks. (E) Quantification of Golgi fragmentation phenotypes in CytoB-treated cultures of WT, *dab^{mz}*, and *Abl* mutants (*df st^{J7}/abl^{l4}*). (F–H) Confocal micrographs of third-instar larval eye imaginal disks, acquired at similar settings, cultured in 10 mM LatD and DMSO-treated mock controls were stained for phalloidin (green), *cis*-Golgi (anti-GM130; red), and anti-Elav (blue). Note the decrease in phalloidin staining at the cortex in LatD-treated cultures compared with mock controls. Single PR cell body is outlined in enlarged panels for the various conditions. Arrowheads represent *cis*-Golgi cisternae. (F) WT. (G) *dab^{mz}*. (H) *Abl* mutant (*Df st^{J7}/abl^{l4}*). Note the random distribution of *cis*-Golgi structures in *dab^{mz}* disks (G) and *Abl* mutant disks (H) compared with WT controls (F) treated with LatD. Scale bar, 5 μ m. (I, J). Quantification of LatD epistasis data. *n* for each treatments is indicated on the bars. Error bars represent SEM. *****p* < 0.001** (estimated by ANOVA). Quantification of fragmentation (I) and basal redistribution (J) of *cis*-Golgi structures after LatD-mediated disruption of actin polymerization in WT, *dab^{mz}*, and *Abl* mutant (*Df st^{J7}/abl^{l4}*) eye disks.

of Golgi cisternae reflects an ongoing balance of fusion and fission events, much as observed previously in yeast (Losev *et al.*, 2006; Matsuura-Tokita *et al.*, 2006). Quantification of these events in wild-type versus *Abl* mutant tissue demonstrated directly that loss of *Abl* significantly increased the frequency of fission events and reduced the frequency of fusions. Second, the absolute volume of *cis*-Golgi in *Abl* mutant photoreceptors was not substantially greater than that in wild type, as judged by direct measurement of the volume of GM130-immunoreactive material in deconvoluted image stacks of photoreceptor clusters. Although we did observe a small apparent increase in Golgi volume in the mutants (~55%, based on pixel counts), we note that Golgi cisternae are small on the length scale of the point spread function of visible light, such that the fluorescence signal from a single cisterna extends into the surrounding cytoplasm. The increase in apparent Golgi volume is therefore within the range expected due simply to fluorescence “spillover” from the threefold greater number of separate Golgi cisternae in the mutants (Schermele *et al.*, 2010).

It is striking that both increase and decrease of Ena led to net fragmentation of Golgi. Why might this be? We know that both fission and fusion of membranes requires actin dynamics: at scission, polymerization provides force for separating membranes, whereas in fusion, actin polymerization is essential for bringing membranes together and for supplying membrane vesicles, among other things (Simlonescu and Pavlath, 2011; Abmayr and Pavlath, 2012). As a result, altering actin dynamics is apt to change the probabilities of multiple aspects of both fission and fusion events, making it impossible to predict *a priori* how the balance will be altered by a given manipulation, just as either increase or decrease of Ena can inhibit cell or axon motility, depending on the details of the experiment, due to the nonlinear nature of actin dynamics (Krause *et al.*, 2002; Trichet *et al.*, 2008). Indeed, in our hands, we also observed net Golgi fragmentation when we stabilized actin with jasplakinolide, just as we did from depolymerization with cytochalasin or latrunculin (R.K. and E.G., unpublished data). More direct experiments will be necessary to fully understand this dynamic.

The effect of *Abl*/Ena signaling was not limited to *cis*-Golgi but also disrupted *trans*-Golgi. Thus we observed changes in both *trans*-Golgi number and localization in *Abl* pathway mutants that mirrored the changes we observed in *cis*-Golgi. It seems likely that the effect of *Abl*/Ena signaling on *cis*-Golgi propagates indirectly to *trans*-Golgi, as we do not observe overt accumulation of Ena on *trans*-Golgi cisternae themselves. Alternatively, at this point we cannot formally rule out a direct effect of *Abl*/Ena signaling on *trans*-Golgi.

There are two basic classes of hypotheses that could account for the effect of *Abl*/Ena signaling on Golgi structure. It could be that Ena binds directly to some Golgi-resident protein, for example, inducing a conformational change that thereby alters the fusion/fission ratio and the subcellular distribution. Alternatively, it could be that *Abl*/Ena signaling regulates Golgi structure more indirectly, by altering actin dynamics, perhaps using the same mechanisms that it uses to control the cortical actin. Our data argue in favor of the latter hypothesis. Our pharmacological experiments show that disrupting actin structure blocks the effect of *Abl* signaling on Golgi distribution, formally placing actin structure downstream of *Abl* in the pathway leading to Golgi biogenesis. Moreover, our genetic experiments showed that simultaneously overproducing both Enabled and actin-capping protein (*cpb*) completely blocked the phenotype of *UAS-ena*. This shows directly that the same actin regulatory mechanism that is the key target of *Abl*/Ena at the cell cortex is also the key target for Golgi regulation. This provides a powerful argument that the fundamental mechanism used by Ena to regulate

Golgi is likely to be the same as that used for the cortical actin cytoskeleton, the anticapping and actin-bundling activities of Enabled.

There is an ongoing debate regarding Golgi dynamics as to whether cargo moves within the Golgi exclusively by packaging in small COPI vesicles or whether larger Golgi units can reassort their contents by cycles of fission and fusion (Patterson *et al.*, 2008; Pfeffer, 2010; Dmitrieff *et al.*, 2013; Lavieu *et al.*, 2013; Marriswood and Warren, 2013; Rizzo *et al.*, 2013). Consistent with the latter idea, large-scale Golgi reassignment has been observed in a couple of cell types, including budding yeast and the *Drosophila* syncytial blastoderm (Frescas *et al.*, 2006). We here, for the first time, observe apparent fission and fusion events of *cis*-Golgi cisternae in identified postmitotic neurons in intact tissue. We emphasize, however, that our live-imaging experiments are limited by the resolution of confocal microscopy, and we have not assessed directly the continuity of the luminal compartments of cisternae before and after apparent fusion events. It will be important in the future to develop and deploy appropriate reagents to test directly for motion of cargo between cisternae.

In the *Drosophila* PR neurons studied here, Enabled is associated with the *cis*-Golgi compartment, but we do not yet know how many other neuronal and nonneuronal cell types will show this association. For example, in primary cultures of vertebrate neurons, Mena controls neuritogenesis by modulating a different step in the secretory process, exocytosis (Gupton and Gertler, 2010; Gupton *et al.*, 2012). It would therefore not be surprising to find Ena associated with the exocytotic machinery rather than the Golgi machinery in this case. Moreover, in *Drosophila* class IV md sensory neurons, secretory deficits selectively disrupt dendritic morphogenesis but not axogenesis, and perhaps consistent with this, *Abl*/Ena function is essential for dendrite arborization in these cells (Li *et al.*, 2005; Shivalkar and Giniger, 2012) but has not been reported to affect their axon patterning. Finally, in some contexts, neuronal development requires local translation of guidance molecules in the growth cone rather than translation in the cell soma (Jung *et al.*, 2011, 2012; Leung *et al.*, 2013). It is likely that the need for actin dynamics to target different subcellular compartments in different cell types will be reflected in different patterns of *Abl*/Ena protein localization.

We report here the role of *Abl*/Ena-dependent regulation of actin structure on overall Golgi structure and localization, but there may be more subtle effects on Golgi function as well. For example, recent evidence supports a role for actin-dependent regulation of the specificity of protein sorting in the Golgi complex (Gomez and Billadeau, 2009; von Blume *et al.*, 2009, 2011; Colon-Franco *et al.*, 2011). Preferential sorting of cargoes is achieved by nucleation of distinct actin filaments at the Golgi complex. In HeLa cells, for example, Arp2/3-mediated nucleation of actin branches at *cis*-Golgi regulates retrograde trafficking of the acid hydroxylase receptor CIMPR (Gomez and Billadeau, 2009), whereas formin family-mediated nucleation of linear actin filaments at Golgi regulates selective trafficking of the lysosomal enzyme cathepsin D (Colon-Franco *et al.*, 2011). Similarly, the actin-severing protein ADF/cofilin, the mammalian orthologue of *Drosophila* twinstar, sculpts an actin-based sorting domain at the *trans*-Golgi network for selective cargo sorting (von Blume *et al.*, 2009, 2011). It will be important to investigate whether the effects of *Abl*/Ena on Golgi morphology have functional consequences on bulk secretion or protein sorting.

Protein trafficking and membrane addition in neurons need to be coordinated with the growth requirements of the axonal and dendritic plasma membranes, but the mechanisms that do so have been obscure (Pulvirenti *et al.*, 2008; Farhan and Rabouille, 2011;

Cancino and Luini, 2013; Mayinger, 2013). Abl pathway proteins associate with many of the ubiquitous guidance receptors that direct axon growth and guidance throughout phylogeny, including Netrin (Forsthoefel *et al.*, 2005), Roundabout (Bashaw *et al.*, 2000), the receptor tyrosine phosphatase DLAR (Wills *et al.*, 1999), Notch (Giniger, 1998; Crouner *et al.*, 2003), and others. Our data therefore suggest a potential link between the regulatory machinery that senses guidance information and the secretory machinery that helps execute those patterning choices. Indeed, preliminary experiments suggest that some of the axonal defects of Abl pathway mutants may arise from alterations in Golgi function (R.K. and E.G., unpublished data). Beyond this, Abl signaling is essential in neuronal migration, epithelial polarity and integrity, cell adhesion, hematopoiesis, and oncogenesis, among other processes (Colicelli, 2010). The data reported here now compel us to reexamine the many functions of Abl to ascertain whether some of these effects arise, at least in part, from regulation of secretory function.

MATERIALS AND METHODS

Fly stocks

Fly sources: GMR-Gal4 on Chr II; Elav-Gal4/Cyo-LacZ on Chr II; C155 Gal4 on Chr I; *dab^{mz}* (Song *et al.* 2010; note that these are molecularly verified *dab* alleles; they are not the misattributed *nrt* alleles identified in prior studies; Liebl *et al.*, 2003); *abl⁴* (D. Van Vactor, Harvard Medical School, Boston, MA); UAS mannII-eGFP (Yuh Nung Jan, University of California, San Francisco, San Francisco, CA); Ye *et al.*, 2007); UAS *cpb*, UAS Ena-GFP, UAS FP4-mito, and UAS AP4-mito (Mark Piefer, University of North Carolina, Chapel Hill, NC); and UAS GRASP65-GFP and UAS Abl-RNAi (#35327) from the Bloomington *Drosophila* Stock Center. Balancer chromosomes with β -galactosidase (β -gal (TM3-*lacZ*, TM6b-T8-*lacZ*, and CyoAct*lacZ*) were used in all experiments.

Immunohistochemistry and phenotypic and statistical analysis: eye imaginal disk

Late third-instar eye imaginal disks with brain lobes were fixed in 4% electron microscopy-grade paraformaldehyde (Electron Microscopy Sciences, Hatfield, PA) in phosphate-buffered saline (PBS) for 30 min. Tissues were blocked for 2 h in blocking mixture containing PBS, 0.3% Triton X-100, 2% goat serum, 2% donkey serum, and 2% bovine serum albumin. All primary antibodies were incubated overnight at 4°C and fluorophore-conjugated secondary antibodies (Jackson ImmunoResearch, West Grove, PA) at 1:250 dilution for 2 h at room temperature. Eye disks with brain lobes were mounted in fluorescence quenching reagent (VectaShield; Bio-Rad, Hercules, CA). Z-sections were collected using an LSM 510 meta-laser scanning confocal microscope (Carl Zeiss MicroImaging, Thornwood, NY) at 63 \times magnification and three dimensionally deconvoluted using AutoQuant software. For any given data, both wild-type and mutant images were analyzed simultaneously with similar threshold settings in Imaris 7.0 (Bitplane, Zurich, Switzerland). The fluorescently labeled, GM130-positive *cis*-Golgi structure and dSyx16-positive *trans*-Golgi structures were analyzed in stack format in Image Pro Plus (Media Cybernetics, Rockville, MD) using a custom-built macro and manually verified before extracting the final numbers for each sample. For presentation, images were projected to a single plane using Imaris 7.0. Colocalization analysis of GM130 and Ena structures was performed using selected individual regions of interest (ROIs), and Pearson's *r* was obtained using Imaris 7.0 Colocalization Threshold module. Final colocalization percentage was derived from an average of independent ROIs derived from various Z-stacks. Statistical significance was assessed by analysis of variance (ANOVA).

The following antibodies were used in this study. Mouse anti-Ena (5G2; 1:50), rat anti-Elav (7E8A10; 1:20), and mouse anti-chaoptin (24B10; 1:100) were from the Developmental Studies Hybridoma Bank (Iowa City, IA). Chicken anti-GFP (1:3000; Aves, Tigard, OR), rabbit anti-GFP (1:1000; Invitrogen, Grand Island, NY), rabbit anti-GM130 (1:100; Abcam, Cambridge, MA), rabbit anti-Syx-16 (1:500; William Trimble, University of Toronto, Canada), rabbit anti-Rab11 (1:100; Donald Ready, Purdue University, West Lafayette, IN), and fluorescein isothiocyanate-phalloidin (1:100; Life Technologies, Grand Island, NY).

Two-color STED microscopy

For STED experiments, the disks were dissected and stained for respective antibodies as described and mounted on Prolong Gold (Molecular Probes, Grand Island, NY) using 22 \times 22-mm Fisherbrand cover glass (No. 1.5; 12-541-B). Two-color STED images were obtained using a commercial Leica TCS STED-CW microscope. A 100 \times /1.4 numerical aperture oil immersion objective lens was used for imaging. We acquired 1024 \times 1024-pixel STED images sequentially line by line with a scan speed of 1000 lines/s with line averaging. Cross-talk between channels was below the noise limit (<5%) as determined by imaging singly labeled samples. Images were deconvoluted using the Leica deconvolution module.

Immuno-electron microscopy

Ultrastructural localization of Ena was performed by preembedding immuno-electron microscopy. Wild-type larvae were individually dissected in PBS and fixed 45 min at room temperature with 4% paraformaldehyde. Permeabilization, labeling, and glutaraldehyde postfixation were then performed as described previously (Tanner *et al.*, 1996), except that saponin was used at 0.2% to permeabilize tissue and at 0.1% in antibody incubations. Anti-Ena was visualized with anti-mouse 1.4-nm Nanogold secondary antibody (1:200 dilution; Nanoprobes, Yaphank, NY). After antibody incubations, tissue was subjected to silver enhancement (HQ kit; Nanoprobes), treatment with osmium tetroxide and uranyl acetate, and dehydration in graded ethanols by standard methods, and eye imaginal disks were isolated by dissection, embedded in epoxy resin, and sectioned. Samples were examined on a JEOL 1200 EX electron microscope using a digital charge-coupled device (CCD) camera.

Live imaging of Golgi dynamics and culturing third-instar larval eye-brain complex for drug epistasis experiments

Late third-instar larvae were washed in sterile PBS to remove fly food and disinfected in 70% ethanol for 2 min. Larvae were then transferred to Schneider's *Drosophila* medium (Life Technologies) supplemented with 2% fetal bovine serum and 0.5% penicillin-streptomycin (15140; Gibco, Grand Island, NY) for dissecting eye-brain complex with fan body. Healthy eye-brain complexes were positioned in 35-mm MatTek culture dishes with glass bottom (P35G-1.5-14-C; MatTek Corporation, Ashland, MA) coated with polylysine (p4832; Sigma-Aldrich, St. Louis, MO) and concanavalin A (C2010; Sigma-Aldrich). After assembly of the culture chamber, fresh culture medium with 0.5 μ g/ml 20-hydroxyecdysone (H5142; Sigma-Aldrich; 500 mg/ml stock solution in 10% isopropanol stored at -20° C) and 1 μ g/ml insulin, human recombinant zinc (4 mg/ml; Life Technologies), was added. The entire assembly was cultured for 1 h at 25°C for drug-induced actin depolymerization experiments using CytoD or LatB (final concentration 20 and 10 μ M, respectively). Control cultures were treated with 0.1% ethanol (for CytoD) and 0.3% dimethyl sulfoxide (DMSO; for LatB). After the culture period,

the samples were fixed, stained with respective primary antibodies, and processed as described.

For live imaging Golgi dynamics, the cultures were imaged in inverted Zeiss spinning disk microscope with electron-multiplying CCD camera at 63× magnification. We used minimal laser power to avoid tissue damage. Typically we collected Z-sections at 1-μm intervals every 0.65 s. The images were three-dimensionally deconvoluted using AutoQuant software and analyzed for Golgi fission and fusion events using the spot tracking module from Image Pro Plus software (Media Cybernetics). Videos were quantified blind to genotype. Statistical significance of all data collected was assessed by ANOVA. Final figures were prepared using Adobe Photoshop CS5, and graphic illustrations were done using Adobe Illustrator CS5.

ACKNOWLEDGMENTS

We thank all the members of our lab for many helpful discussions during the course of this work. We are also grateful to Chi-Hon Lee and Chun-Yuan Ting for their help with analysis of photoreceptor development. For comments on the manuscript, we are grateful to Craig Blackstone, Frank Gertler, and Mark Peifer. Antibodies and fly stocks were generously provided by Donald Ready for anti-Rab11, Bing Ye (University of Michigan, Ann Arbor, MI) for Golgi markers, and William Trimble for anti-dSyx-16. We gratefully acknowledge the excellent technical assistance of Joy Gu in preparing samples for immuno-electron microscopy and also of Carolyn Smith (National Institute of Neurological Disorders and Stroke Light Imaging Facility) and Susan Cheng and Virginia Crocker (National Institute of Neurological Disorders and Stroke Electron Microscopy Facility). These experiments were supported by the Basic Neuroscience Program of the National Institute of Neurological Disorders and Stroke Intramural Research Program, National Institutes of Health, Grant Z01-NS003013 to E.G. S.H.N. was supported by National Institutes of Health Grant GM47857 to Mark Peifer. S.W. was supported by the intramural program of the National Human Genome Research Institute.

REFERENCES

Abmayr SM, Pavlath GK (2012). Myoblast fusion: lessons from flies and mice. *Development* 139, 641–656.

Almeida CG, Yamada A, Tenza D, Louvard D, Raposo G, Coudrier E (2011). Myosin 1b promotes the formation of post-Golgi carriers by regulating actin assembly and membrane remodeling at the trans-Golgi network. *Nat Cell Biol* 13, 779–789.

Anitei M, Stange C, Parshina I, Baust T, Schenck A, Raposo G, Kirchhausen T, Hoflack B (2010). Protein complexes containing CYFIP/Sra/PIR121 coordinate Arf1 and Rac1 signalling during clathrin-AP-1-coated carrier biogenesis at the TGN. *Nat Cell Biol* 12, 330–340.

Aridor M, Fish KN (2009). Selective targeting of ER exit sites supports axon development. *Traffic* 10, 1669–1684.

Bashaw GJ, Kidd T, Murray D, Pawson T, Goodman GS (2000). Repulsive axon guidance: Abelson and Enabled play opposing roles downstream of the roundabout receptor. *Cell* 101, 703–715.

Bear JE, Svitkina TM, Krause M, Schafer DA, Loureiro JJ, Strasser GA, Maly IA, Chago OY, Cooper JA, Borisy GG (2002). Antagonism between Ena/VASP proteins and actin filament capping regulates fibroblast motility. *Cell* 109, 509–521.

Bradley WD, Koleske AJ (2009). Regulation of cell migration and morphogenesis by Abl family kinases: emerging mechanisms and physiological contexts. *J Cell Sci* 122, 3441–3454.

Camera P, da Silva JS, Griffiths G, Giuffrida MG, Ferrara L, Schubert V, Imarisio S, Silengo L, Dotti GG, Di Cunto F (2003). Citron-N is a neuronal Rho-associated protein involved in Golgi organization through actin cytoskeleton regulation. *Nat Cell Biol* 5, 1071–1078.

Cancino J, Luini A (2013). Signaling circuits on the Golgi complex. *Traffic* 14, 121–134.

Colicelli J (2010). ABL tyrosine kinases: evolution of function, regulation and specificity. *Sci Signal* 139, 1–26.

Colon-Franco JM, Gomez TS, Billadeau DD (2011). Dynamic remodeling of the actin cytoskeleton by FMNL1γ is required for structural maintenance of the Golgi complex. *J Cell Sci* 124, 3118–3126.

Comer AR, Ahern-Djamali SM, Juang JL, Jackson PD, Hoffmann FM (1998). Phosphorylation of Enabled by the *Drosophila* Abelson tyrosine kinase regulates the *in vivo* function and protein-protein interactions of Enabled. *Mol Cell Biol* 18, 152–160.

Crowner D, Le Gall M, Gates MA, Giniger E (2003). Notch steers *Drosophila* ISNb motor axons by regulating the Abl signaling pathway. *Curr Biol* 13, 967–972.

Dmitrieff S, Rao M, Sens P (2013). Quantitative analysis of intra-Golgi transport shows inter-cisternal exchange for all cargo. *Proc Natl Acad Sci USA* 110, 15692–15697.

Egea G, Lazaro-Dieguez F, Vilella M (2006). Actin dynamics at the Golgi complex in mammalian cells. *Curr Opin Cell Biol* 18, 168–178.

Farhan H, Rabouille C (2011). Signaling to and from the secretory pathway. *J Cell Sci* 15, 171–180.

Forsthoefel DJ, Liebl EC, Kolodziej PA, Seeger MA (2005). The Abelson tyrosine kinase, the Trio GEF and Enabled interact with the Netrin receptor Frazzled in *Drosophila*. *Development* 132, 1983–1994.

Frescas D, Mavrakis M, Lorenz H, Delotto R, Lippincott-Schwartz J (2006). The secretory membrane system in the *Drosophila* syncytial blastoderm embryo exists as functionally compartmentalized units around individual nuclei. *J Cell Biol* 173, 219–230.

Gates J, Mahaffey JP, Rogers SL, Emerson M, Rogers EM, Sottile SL, Van Vactor D, Gertler FB, Peifer M (2007). Enabled plays key roles in embryonic epithelial morphogenesis in *Drosophila*. *Development* 134, 2027–2039.

Gates J, Nowotarski SH, Yin H, Mahaffey JP, Bridges T, Herrera C, Homem CCF, Janody F, Montell DJ, Peifer M (2009). Enabled and Capping protein plays important roles in shaping cell behavior during *Drosophila* oogenesis. *Dev Biol* 333, 90–107.

Gertler F, Doctor J, Hoffman F (1990). Genetic suppression of mutations in the *Drosophila abl* proto-oncogene homolog. *Science* 248, 857–860.

Giniger E (1998). A role for *abl* in *Notch* signaling. *Neuron* 20, 667–681.

Gomez TS, Billadeau DD (2009). A FAM21-containing WASH complex regulates retromer-dependent sorting. *Dev Cell* 17, 699–711.

Grevengoed E, Fox DT, Gates J, Peifer M (2003). Balancing different types of actin polymerization at distinct sites: roles for Abelson kinase and Enabled. *J Cell Biol* 163, 1267–1279.

Grevengoed E, Loureiro J, Jesse T, Peifer M (2001). Abelson kinase regulates epithelial morphogenesis in *Drosophila*. *J Cell Biol* 155, 1185–1197.

Gu JJ, Lavau CP, Pugacheva E, Soberblom EJ, Moseley MA, Pendergast AM (2012). Abl family kinases modulate T cell-mediated inflammation and chemokine-induced migration through the adaptor HEF1 and the GTPase Rap1. *Sci Signal* 17, ra51.

Gupton FL, Gertler FB (2010). Integrin signaling switches the cytoskeletal and exocytic machinery that drives neurogenesis. *Dev Cell* 18, 725–736.

Gupton FL, Riquelme D, Huges-Alford SK, Tadros J, Rudina SS, Hynes RO, Lauffenburger D, Gertler FB (2012). Mena binds α5 integrin directly and modulates α5β1 function. *J Cell Biol* 198, 657–676.

Hansen SD, Mullins RD (2010). VASP is a processive actin polymerase that requires monomeric actin for barbed end association. *J Cell Biol* 191, 571–584.

Herskowitz I (1987). Functional inactivation of genes by dominant negative mutations. *Nature* 329, 219–222.

Homem CCF, Janody F, Montell DJ, Peifer M (2009). Enabled and Capping protein play important roles in shaping cell behavior during *Drosophila* oogenesis. *Dev Biol* 333, 90–107.

Jung H, O'Hare CM, Holt CE (2011). Translational regulation in growth cones. *Curr Opin Genet Dev* 21, 458–464.

Jung H, Yoon BC, Holt CE (2012). Axonal mRNA localization and local protein synthesis in nervous system assembly, maintenance and repair. *Nat Rev Neurosci* 13, 308–324.

Kondylis V, Panzerden HE, Herpers B, Friggi-Grelin F, Rabouille C (2007). The Golgi comprises a paired stack that is separated at G2 by modulation of the actin cytoskeleton through Abi and Scar/WAVE. *Dev Cell* 12, 901–915.

Kondylis V, Rabouille C (2003). A novel role for dp115 in the organization of tER sites in *Drosophila*. *J Cell Biol* 162, 185–198.

- Kondylis V, Rabouille C (2009). The Golgi apparatus: lessons from *Drosophila*. *FEBS Lett* 583, 3827–3838.
- Krause M, Bear JE, Loureiro JJ, Gertler FB (2002). The Ena/VASP enigma. *J Cell Sci* 115, 4721–4726.
- Kuzina I, Song JK, Giniger E (2011). How Notch establishes longitudinal axon connections between successive segments of the *Drosophila* CNS. *Development* 138, 1839–1849.
- Lavieu G, Zheng H, Rothman JE (2013). Stapled Golgi cisternae remain in place as cargo passes through the stack. *eLife* 2, e00558.
- Leung LC, Urbancic V, Baudet ML, Dwivedy A, Bayley TG, Lee AC, Harris WA, Holt CE (2013). Coupling of NF-protocadherin signaling to axon guidance by cue-induced translation. *Nat Neurosci* 16, 166–173.
- Li W, Li Y, Gao FB (2005). Abelson, Enabled, and p120 catenin exert distinct effects on dendritic morphogenesis in *Drosophila*. *Dev Dyn* 234, 512–522.
- Liebl EC, Forsthoefel DJ, Franco LS, Sample SH, Hess JE, Cowger J, Chandler MP, Shupert AM, Seeger MA (2000). Dosage-sensitive, reciprocal genetic interactions between the Abl tyrosine kinase and the putative GEF trio reveal trio's role in axon pathfinding. *Neuron* 26, 107–118.
- Liebl EC, Rowe RG, Forsthoefel DJ, Stammier AL, Schmidt ER, Turski M, Seeger MA (2003). Interactions between the secreted protein Amalgam, its transmembrane receptor Neurotactin and the Abelson tyrosine kinase affect axon pathfinding. *Development* 130, 3217–3226.
- Losev E, Reinke CA, Jellen J, Strongin DE, Bevis BJ, Glick BS (2006). Golgi maturation visualized in living yeast. *Nature* 441, 1002–1006.
- Lowery LA, Lee H, Lu C, Murphy R, Obar RA, Zhai B, Schedl M, Van Vactor D, Zhan Y (2010). Parallel genetic and proteomic screens identify Msps as a CLASP-Abl pathway interaction in *Drosophila*. *Genetics* 185, 1311–1325.
- Marriswood B, Warren G (2013). Stalemate in the Golgi battle. *Science* 341, 1465–1466.
- Matas OB, Martinez-Menarguez JA, Egea G (2004). Association of Cdc42/N-WASP/Arp2/3 signaling pathway with Golgi membranes. *Traffic* 5, 838–846.
- Matsuura-Tokita K, Takeuchi M, Ichihara A, Mikuriya K, Nakano A (2006). Live imaging of yeast Golgi cisternal maturation. *Nature* 441, 1007–1010.
- Mayinger P (2013). Signaling at the Golgi. *Cold Spring Harb Perspect Biol* 1, a005314.
- Ori-McKenney KM, Jan LY, Jan YN (2012). Golgi outposts shape dendrite morphology by functioning as sites of centrosomal microtubule nucleation in neurons. *Neuron* 76, 921–930.
- Papoulas O, Hays TS, Sisson JC (2005). The Golgin Lava lamp mediates dynein-based Golgi movements during *Drosophila* cellularization. *Nat Cell Biol* 7, 612–618.
- Patterson GH, Hirschberg K, Polishchuk RS, Gerlich D, Phair RD, Lippincott-Schwartz J (2008). Transport through the Golgi apparatus by rapid partitioning within a two-phase membrane system. *Cell* 133, 1055–1067.
- Pfeffer SR (2010). How the Golgi works: a cisternal progenitor model. *Proc Natl Acad Sci USA* 107, 19614–19618.
- Pulvirenti T, Giannotta M, Capestrano M, Capitani M, Pisanu A, Polishchuk RS, San Pietro E, Benzoussenko GV, Mironoc AA, Turacchio G, et al. (2008). A traffic-activated Golgi-based signaling circuit coordinates the secretory pathway. *Nat Cell Biol* 10, 912–922.
- Rizzo R, Parashuraman S, Mirabelli P, Puri C, Lucocq J, Luini A (2013). The dynamics of engineered resident proteins in the mammalian Golgi complex relies on cisternal maturation. *J Cell Biol* 201, 1027–2036.
- Rosso S, Bollati F, Bisbal M, Peretti D, Sumi T, Nakamura T, Quiroga S, Ferreira A, Caceres A (2004). LIMK1 regulates Golgi dynamics, traffic of Golgi-derived vesicles and process extension in primary cultured neurons. *Mol Biol Cell* 15, 3433–3449.
- Salvareza SB, Deborde S, Schreiner R, Campagne F, Kessels MM, Qualmann B, Caceres A, Kreitzer G, Rodriguez-Boulan E (2009). LIM kinase 1 and cofilin regulate actin filament population required for dynamin-dependent apical carrier fission from the trans-Golgi network. *Mol Biol Cell* 20, 438–451.
- Schermelleh L, Heintzmann R, Leonhardt H (2010). A guide to super-resolution fluorescence microscopy. *J Cell Sci* 19, 165–175.
- Shivalkar M, Giniger E (2012). Control of dendritic morphogenesis by Trio in *Drosophila melanogaster*. *PLoS ONE* 7, 1–10.
- Simlonescu A, Pavlath GK (2011). Molecular mechanisms of myoblast fusion across species. *Adv Exp Med Biol* 713, 113–135.
- Song JK, Giniger E (2011). Noncanonical Notch function in motor axon guidance is mediated by Rac GTPase and the GEF1 domain of trio. *Dev Dyn* 240, 324–332.
- Song JK, Kannan R, Merdes G, Singh J, Mlodzik M, Giniger E (2010). Disabled is a bona fide component of the Abl signaling network. *Development* 137, 3719–3727.
- Tanner V, Ploug T, Tao-Cheng J-H (1996). Subcellular localization of SV2 and other secretory vesicle components in PC12 cells by an efficient method of pre-embedding EM immunocytochemistry for cell cultures. *J Histochem Cytochem* 144, 1481–1488.
- Tong C, Ohyama T, Tien A, Rajan A, Haueter C, Bellen HJ (2011). Rich regulates target specificity of photoreceptor cells and N-cadherin trafficking in the *Drosophila* visual system via Rab6. *Neuron* 71, 447–459.
- Trichet L, Sykes C, Plastino J (2008). Relaxing the actin cytoskeleton for adhesion and movement with Ena/VASP. *J Cell Biol* 181, 19–25.
- Valderrama F, Luna A, Babia T, Martinez-Menarguez JA, Ballesta J, Barth H, Chaponnier C, Renau-Piqueras J, Egea G (2000). The Golgi-associated COP1-coated buds and vesicles contain beta/gamma-actin. *Proc Natl Acad Sci USA* 97, 1560–1565.
- von Blume J, Alleaume AM, Cantero-Recasens G, Curwin A, Carreras-Sureda A, Zimmermann T, van Galen J, Wakana Y, Valverde MA, Malhotra V (2011). ADF/Cofilin regulates secretory cargo sorting at the TGN via the Ca²⁺ ATPase SPCA1. *Dev Cell* 20, 652–662.
- von Blume J, Duran JM, Forlanelli E, Alleaume AM, Egorov M, Polishchuk R, Molina H, Malhotra V (2009). Actin remodeling by ADF/cofilin is required for cargo sorting at the trans-Golgi network. *J Cell Biol* 187, 1055–1069.
- Wills Z, Bateman J, Korey CA, Comer A, Van Vactor D (1999). The tyrosine kinase Abl and its substrate Enabled collaborate with the receptor phosphatase Dlar to control motor axon guidance. *Neuron* 22, 301–312.
- Xu H, Boulianne GL, Trimble WS (2002). *Drosophila* Syntaxin 16 is a Q-SNARE implicated in Golgi dynamics. *J Cell Sci* 115, 4447–4455.
- Ye B, Ye Y, Zhang W, Song S, Younger H, Jan LY, Jan YN (2007). Growing dendrites and axons differ in their reliance on the secretory pathway. *Cell* 130, 717–729.
- Zuber C, Spiro MJ, Guhl B, Spiro RG, Roth J (2000). Golgi apparatus immunolocalization of endomannosidase suggests post-endoplasmic reticulum glucose trimming: implications for quality control. *Mol Biol Cell* 11, 4227–4240.